Biomedical Signal Processing and Control 75 (2022) 103582

Contents lists available at ScienceDirect

Biomedical Signal Processing and Control

journal homepage: www.elsevier.com/locate/bspc

A lightweight and accurate double-branch neural network for four-class motor imagery classification

Weifeng Ma *, Yifei Gong, Haojie Xue, Yang Liu, Xuefen Lin, Gongxue Zhou, Yaru Li

School of Information and Electronic Engineering, Zhejiang University of Science and Technology, Hangzhou 310023, People's Republic of China

ARTICLE INFO

Keywords:
Brain-computer interfaces (BCIs)
Electroencephalography (EEG)
Motor imagery (MI)
Deep learning
Feature fusion

ABSTRACT

Deep learning is an important pathway for investigation of motor imagery signal classification. Nevertheless, maintaining a good compromise between performance and computational cost has been a major challenge in developing deep models for decoding motor imagery EEG. In this paper, a novel shallow double-branch convolutional neural network (DSCNN) is proposed for four-class motor imagery classification. The proposed CNN adopts parallel extraction of two branches to improve classification accuracy. Meanwhile, in order to constrain the depth of the whole network, the left branch only contained two single temporal and spatial convolutional layers to extract common EEG features. Similarly, the right branch first introduced 1D convolution to exploit the channel dependency and temporal features across multiple time-scales, secondly a depth-wise separable convolutional layer was applied for optimizing EEG signal series. Then the feature representation for final classification was obtained by merging intermediate features extracted from the two branches. Also, the DSCNN is an end-to-end decoder, as it employs the raw EEG data as inputs and does not require additional complex preprocessing. The proposed model was evaluated on public benchmark BCI competition IV dataset 2a and achieved in terms of accuracy is 85% and kappa value is 0.79. Compared with other state-of-the-art algorithms, the experiment results reveal that the DSCNN has higher decoding accuracy and robustness, as well as a 10% improvement in accuracy than the single general shallow model. Furthermore, as a lightweight architecture, the DSCNN relies on a lower computational power than similar mainstream models, which is more in line with the requirements of low delay and real-time performance in practical BCI applications.

1. Introduction

Brain-computer interface (BCI) system makes biomedical signals EEG not limited to being applied to clinical, and is widely used as a reliable control signal to connect the human brain and external devices [1–3]. Spontaneous and evoked EEG signals lead come different BCIs [4]. Among them, BCI based on motor imagery EEG are popular for more general application scenarios in fields such as robotic control and disability assistance [5–8]. This type of electric signal is caused by the activation of neurons in specific areas of the brain from the imagining of body movement, and it is accompanied by ERS/ERD [9], which is the key to driving the classification of motor imagery EEG signals. Based on this, classical machine-learning algorithms extract features related with ERS/ERD from signals of trials and then classify. A large number of algorithms that relied on time-frequency analysis were proposed to study the energy changes due to ERS/ERD [10]. Furthermore, common spatial pattern (CSP) and its derivative improved algorithms obtained satisfactory results on different datasets and were considered one of the most common EEG pattern recognition methods [11,12].

However, there are serious individual differences in motor imagery EEG signals from different subjects, and the degree of ERS/ERD caused by different subjects is also different [13–15]. For the same motor imagery, the classification information is distributed in different time domain, frequency domain and spatial domain of EEG signals. Additionally, recorded EEG signals are not pure and usually mixed with noise and artifacts, as a result, traditional feature extraction methods mainly rely on the design of prior knowledge are unable to meet the needs of high-precision classification tasks and the commonly adopted linear classifier as well as SVM can not fit the non-stationary EEG signals effectively, which also further restricts the decoding performance of the model. In order to reduce the defects caused by the handcrafted extraction features, neural network based on deep learning has become a powerful tool for EEG decoding because it can automatically extract features and classify.

* Corresponding author.
E-mail address: mawf@zust.edu.cn (W. Ma).

https://doi.org/10.1016/j.bspc.2022.103582
Received 29 September 2021; Received in revised form 12 January 2022; Accepted 12 February 2022

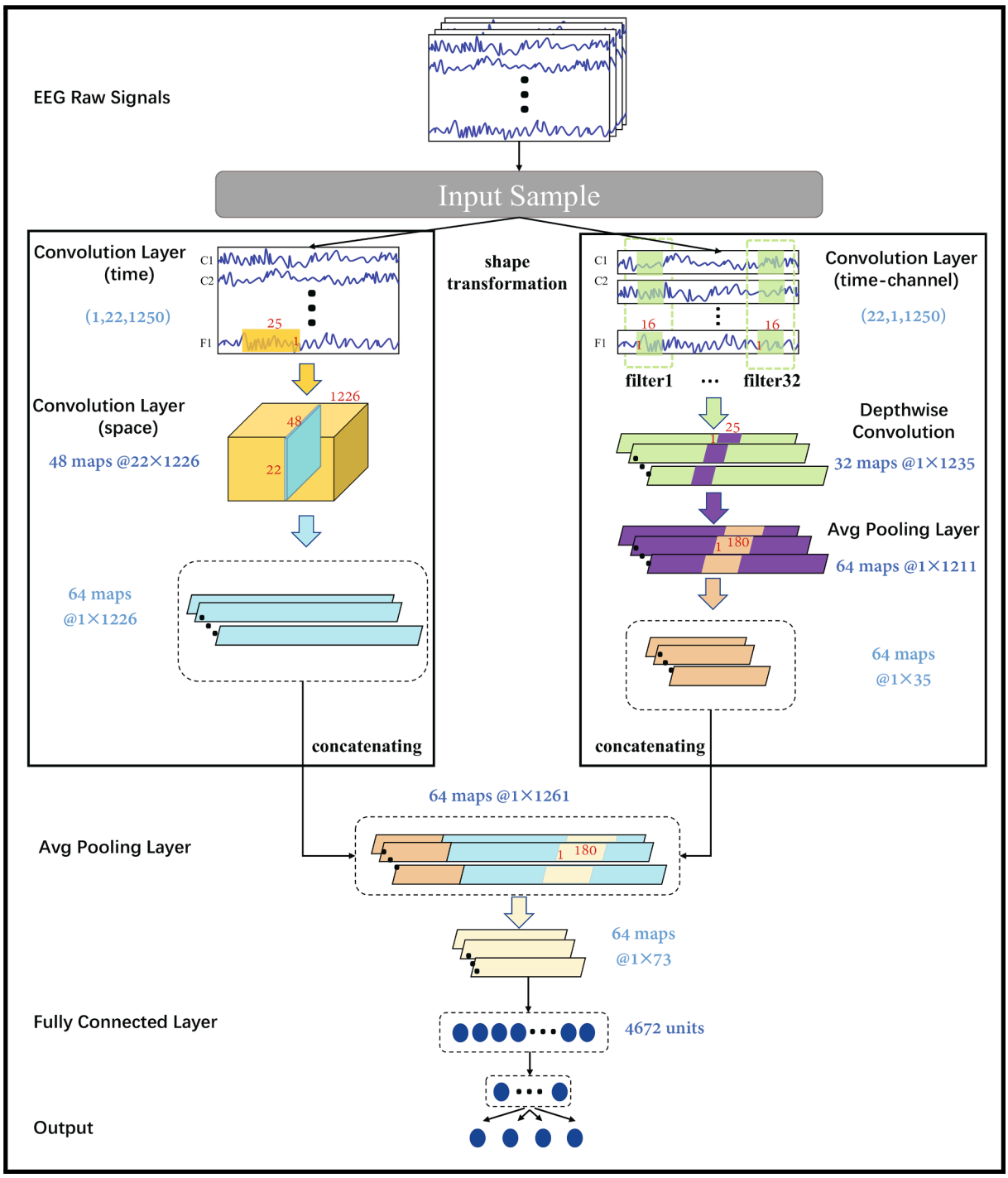

Fig. 1. An schematic illustration of the DSCNN overall architecture, where the color of feature maps denotes which convolutional layer or module it comes from. The branches of the model is described in the form of left and right. In detailed, the shape transformation layer is functioned on the right branch for transforming the same input EEG trial sample as the left branch.

Recently, the widespread use of deep learning in intersecting fields has proved that this technology has enough potential. Therefore, the researchers borrowed the deep learning frameworks proposed in computer vision and natural language processing and introduced them into the pattern recognition of EEG signals. Compared to traditional machine-learning methods, the classification accuracy improved by more than 5%. In terms of feature extraction, the feature representation learning of images and time series by convolution neural network (CNN) and recurrent neural network (RNN) is also applicable to EEG signal series, which makes the learned features in time domain, frequency domain and spatial domain more diverse and rich, and are matched with ERS/ERD phenomenon. However, both CNN and RNN need to introduce huge trainable parameters to support network calculation when fitting multi-channel EEG data. Although the classification accuracy can be significantly improved by extending the network depth longitudinally, EEG datasets are usually small labeled, which leads the deep network to easily causing vanishing gradient or exploding gradient and overfitting during training. Importantly, a slight accuracy improvement requires a lot of time and space resources. Therefore, the current existing models generally use a lightweight shallow architecture, but the decoding

performance of these approaches is mostly maintained between 70% and 80% without taking into account the robustness.

In order to maintain a good compromise between accuracy and parsimony, this paper proposes a novel shallow CNN model called double-branch convolutional neural network (DSCNN). It adopts parallel extraction to increase the network's width, each branch introduces very few convolution layers, which effectively reduces the negative impact of the stacking network depth, meanwhile, greatly improves the classification accuracy of the four-class MI tasks.

2. Related work

For classical machine learning algorithms, MI feature extraction attempts to maximize the representation of ERS/ERD phenomena in the time domain, frequency domain and spatial domain of EEG signals. Wavelet transforms (WT) and short-time Fourier transforms (STFT) are usually used to construct time-frequency representations containing EEG feature information [16–18]. However, the resolution of the time-frequency transform is determined for the final classification. This impact will be amplified by individual differences in EEG during ERD or ERS detection. For low SNR (signal-noise-ratio) EEG signals, time-frequency domain features are incomplete for decoding. In fact, the differences between EEG signals from different channels are related to the spatial distribution of channels. Hence, signals from adjacent channels tend to be more similar in the time and frequency domains [19]. G. Pfurtscheller et al. proposed a bank of spatial filters to find these most distinctive spatial features, their method was called CSP and proved its effective on binary classification tasks [11]. Furthermore, K.K. Ang and Aghaei et al. put forward improved algorithms FBCSP and SCSSP based on CSP, which not only achieved higher classification accuracy but also reduced computational cost [20,21].

Although the aforementioned classical algorithms improve the classification accuracy to 70% and are suitable for high-speed brain-computer interface applications, these approaches greatly affected by individual EEG differences and the weak robustness leads to extremely low decoding accuracy for some subjects. In addition, complex and inefficient feature extraction hinders the improvement of classification accuracy. In order to further improve the decoding performance of brain-computer interfaces, deep neural networks make separate feature extraction and classification into a single process and learn the feature representations related to ERD/ERS phenomena by training [22,23].

Common EEG decoding networks usually adopt CNN containing two layers temporal and spatial convolutional layers to extract EEG features in time and space dimension respectively. This shallow architecture was proposed by Schirrmeister et al. and gradually became the general paradigm of EEG decoding in CNN [24]. Lawhern et al. also proposed a systematic decoding framework EEGNet which can be across different BCI paradigms and introduce depthwise separable convolution to deal with the individual difference of EEG features [25]. In Sakhavi's work, in order to reduce the amount of trainable parameters, the EEG signals were classified by the designed CNN after being pre-processed and downsampled by FBCSP [26]. Farahat proposed a branch CNN model which expanded the network's depth and width by stacking more convolutional layers to extract different level EEG features [27]. Zhao et al. proposed a deep learning framework M3DCNN based on multi-branch 3D convolutional neural network by introducing a new 3D representation of EEG and proved that this method can extract more EEG spatial features than common 2D convolution [19]. Y. Li et al. proposed a channel-projection mixed-scale CNN decoding framework CP-MixedNet and introduced a bank of 1D filters to exploit the spatial dependency and temporal features, which is different from the previous approach using multi-dimensional convolution (2D or 3D) [28]. Furthermore, in order to extract more rich and high-level multi-dimensional EEG features, according to Amin's work, a multi-layer CNNs model MCNN including different depth of single CNN was trained to extract the time and space domain features at different convolution kernel scales [29]. R. L. Zhang et al. introduced RNN and proposed a novel hybrid deep learning scheme CNN-LSTM and the classification accuracy reached 84% under four-class task [14]. In addition, C. Zhang et al. proposed a deep convolutional neural network EEG-Inception model stacking Inception and Residual modules from computer vision field for motor imagery EEG decoding, which augments the EEG data by adding candidate noise to the sample and achieved a high accuracy of 88.39% and has strong robustness [30]. G. Dai et al. made use of the information of different frequency bands of raw EEG signals and employ them as multiple inputs, and proposed a HS-CNN with hybrid convolution scale for EEG decoding. The classification accuracy reached 87.6% after the new EEG signals were generated by being reconstructed frequency domain [13].

Based on the previous works, we found that the shallow neural network can meet the requirements of high-speed classification in practice applications, but the accuracy cannot be guaranteed, while deep or hybrid models get higher decoding accuracy and robustness at the cost of computation and resource consumption. Therefore, our main work in this paper is to build a balance based on the above two points to obtain a satisfactory decoding performance with a low resource cost, which can be carried by real BCI systems.

3. The proposed network architecture

This section describes the proposed branch network model. The architecture and overall workflow of the entire model are shown in Fig. 1.

3.1. Pre-processing

Since our proposed DSCNN model applies raw EEG data as input, it does not require additional complex EEG preprocessing. Following the principle of minimal preprocessing, on the one hand, the impact of noise and artifacts in EEG signals should be minimized, and on the other hand, to prevent the loss of key feature information. Hence, a 3rd-order Butterworth bandpass filter of 4∼38 Hz was applied to preprocess the each EEG trial of the interested frequency band related to the subject of motor imagery. In addition, we abandoned the stage of smoothing the EEG signals. Although this can decrease glitch power and oscillations in the EEG signals, it will also hinder the network from learning noise.

3.2. Shallow double-branch neural network(DSCNN)

The proposed network adopts a dual-branch parallel strategy to extract features and both the left branch and the right branch can operate as independent decoding models (see **Fig. 1**).

3.2.1. Network overview

In order to construct a branch model to extract different levels of EEG features in parallel, the left and right branches are fed with different shapes of the same EEG trial samples. When the network executes a workflow, the multi-channel raw EEG signals are preprocessed and then divided into a single trial of batches as training input samples. Second, the EEG trial sample with the shape of (1,22,1250) is fed into the left branch, meanwhile, the shape of the trial is permutated from (1,22,1250) to (22,1,1250) by shape transformation layer and then fed to the right branch. Subsequently, the branch model extracts features from the width (parallel extraction), the feature maps obtained from the two branches are concatenated and then used as the intermediate representation of the final EEG features for classification.

3.2.2. Branch-left

The left branch is designed to extract the temporal and spatial feature representations of EEG signals. The first two layers are individual convolutional layers for convolving along different dimensions of the EEG signal. In the first stage, the number of 48 temporal convolutional kernels with the shape of 1×25 extract the time domain feature representation along the time dimension of EEG signals. In the second stage,

Table 1
The detail of the architecture of proposed double-branch CNN.

Layer Type	Number of Filters	Output Shape (channel*height*width)	Kernel Size	Stride	parameters
Input layer					
Branch-Left		$1 \times 22 \times 1250$			
Branch-Right		$22 \times 1 \times 1250$			
1st convolutional layer					
Branch-Left	48	$48 \times 22 \times 1226$	1×25	1×1	1248
Branch-Right(1D)	32	$32 \times 1 \times 1235$	16	1	11264
2nd convolutional layer					
Branch-Left	64	$64 \times 1 \times 1226$	22×1	1×1	67648
Branch-Right	64	$64 \times 1 \times 1211$	1×25	1×1	1664
Local avg pooling layer					
Branch-Right	64	$64 \times 1 \times 35$	$64 \times 1 \times 180$	1×30	
Global avg pooling layer	64	$64 \times 1 \times 73$	$64 \times 1 \times 180$	1×15	
Fallten layer		4672			
Full connected layer		4			18688

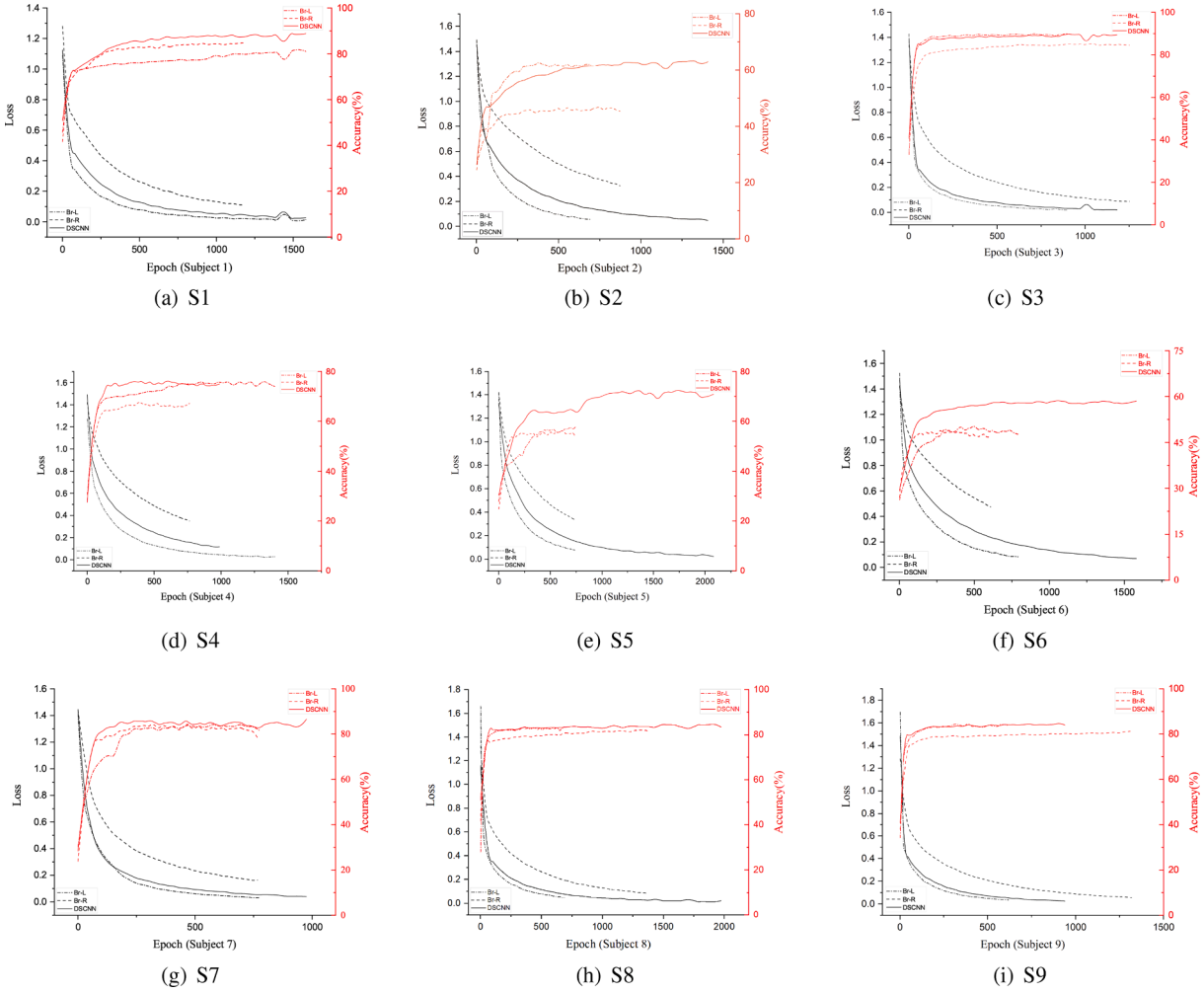

(a) S1 (b) S2 (c) S3

(d) S4 (e) S5 (f) S6

(g) S7 (h) S8 (i) S9

Fig. 2. The training errors and test accuracies of all the nine subjects during epochs.

the spatial convolutional layer of 64 filters with the size of 22×1 convolve along the channel dimension of the temporal feature maps with shape of $(48, 22, 1226)$. The final obtained 64 single channel time series with a length of 1226 represent the intermediate feature extracted by the left branch. In fact, we hope that the entire parallel model maintains a shallow architecture and introduces fewer trainable parameters. Hence, each branch model needs to control the number of layers. For this reason, the first two layers of the left branch follow the convolution paradigm of the shallow model ShallowNet proposed by Schirrmeister [24]. A single temporal and spatial convolutional layer is created to extract the time and space domain feature representation of the EEG signals, which effectively constrains the depth of the branch model.

3.2.3. *Branch-right*

It is incomplete to use only the intermediate features extracted from the left branch model to obtain high-precision decoding performance. In order to obtain richer and higher levels of EEG features for the final

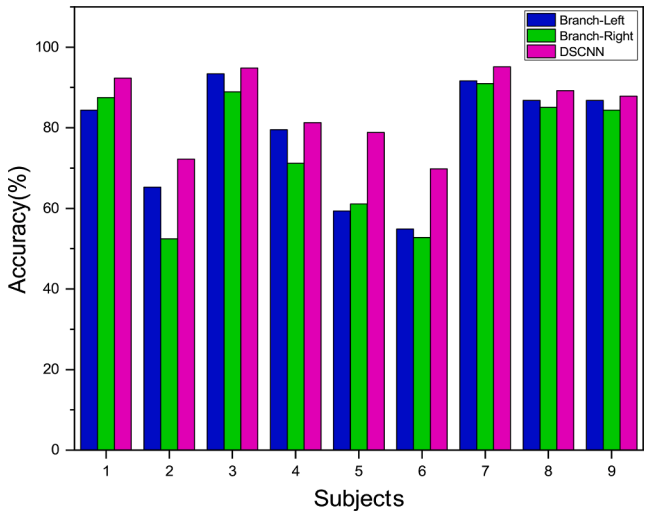

Fig. 3. The accuracy results of classification by two branches and DSCNN.

Table 2
Parameters Summary.

Module	Number of parameters
Branch-Left	69,024
Branch-Right	13,056
Total Parameters	100,704
Trainable Parameters	100,704
Total Size(MB)	0.38

Table 3
Wilcoxon signed-rank test between proposed DSCNN and two branches.

Models	Branch-Left	Branch-Right
P-values	0.018	0.002

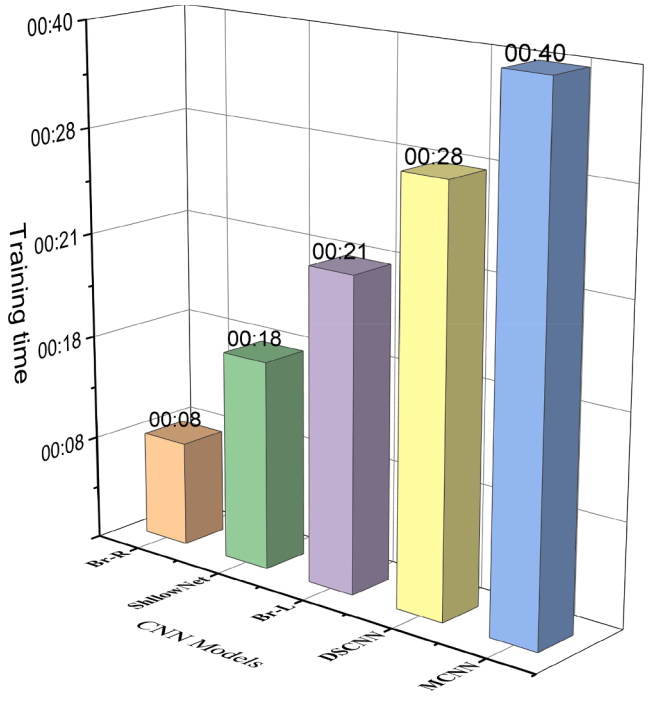

Fig. 4. Average training time per subject in **(h:mm)** for different CNN models.

classification, and to complement the left branch, the right branch is developed to exploit the channel dependency and temporal features across multiple time-scales [31]. The shape of the EEG trial after transformed is $(22,1,1250)$, compared with the feature maps fed into the left branch, theses EEG channel series are allowed from a single channel convolution to a multi-channel convolution. Therefore, we constructed a bank of 1D filters including 32 kernels with the size of 16, convolving across all EEG channels, which makes the multi-channel EEG series with the shape of $(32,1,1235)$ generated by this layer equal to the linearly combined output of the all raw EEG feature channels after multi-channel convolution. Then the depthwise separable convolution with kernel size of 1×25 is introduced and convolve along the time dimension of these mixed signal series for obtaining higher-level channel-time features. Compared with regular convolution, depthwise separable convolution is better at optimizing and merging the output of internal and across feature maps, and can reduce trainable parameters when training [25,32,33]. In addition, the kernel maximum norm constraint is used in this layer. In the following, a local average pooling layer is applied to further downsample along the time dimension of feature maps within the branch for reducing the length of the EEG signal series. The intermediate EEG feature signals retained by the right branch are much shorter in length (length is 35), which is to avoid generating too long EEG feature signal series after fusion with the output of the left branch.

3.2.4. Concatenation and classification

After both the left and right branches finished the extraction in parallel, the respective intermediate features were aggregated into a new EEG channel feature series with the shape of $(64,1,1261)$. These feature maps were sampled by a global average pooling layer with the pool size of 180, allowing extraction of averaged mixed features' activations of 720 ms, and were used for the final classification of the entire model. Before the soft-max classifier, these 2D feature representations were flattened to an 1D vector and then fed into the fully connected layer. The proposed model adopts Exponential Linear Units (ELUs) to speed up the network's convergence and improve the noise-robust learning of ability when fitting non-stationary EEG data [34]. Additionally, in order to prevent overfitting, Batch normalization and Dropout techniques were used [35,36]. The main parameters of the proposed DSCNN architecture are given in **Table 1**.

3.3. Training strategy

We use the BrainDecode framework proposed by Schirrmeister to implement the training of the DSCNN. The model is accelerated training by Nvidia GeForce RTX 2060. In order to ensure the model is converged, early stopping technique was applied to determine the final epoch to stop. When there is no improvement in the test accuracy of a number of epochs or the total iteration exceeds the preset maximum value, the training is stopped. In this experiment, the maximum number of patience increase epoch is 500, and the maximum total iteration allowed is set to 2500 epochs. Although the DSCNN model is a branch model, the branch modules Branch-Left and Branch-Right share the global loss function in the training process. The loss function used in this experiment is the binary-class cross-entropy function:

$$H_p(q) = -\frac{1}{N}\sum_{i=1}^{N} y_i \cdot \log(p(y_i)) + (1-y_i)\cdot\log(1-p(y_i)) \quad (1)$$

where y is the target label, $p(y)$ is the probability that a given EEG trial sample belongs to this label predicted by the model, and N is the total sample size. In addition to adopting the backpropagation algorithm to update the weights of the neural network, the ADAM optimizer was introduced to speed up the correction of the loss function.

Also, in this study, the 5s period of EEG trial after the cue was selected as the training input data. Here, we totally used 288 trials as a training set to train a specific-subject model for per subject. The training

Table 4
Comparison of total number of trainable parameters on dataset BCI IV 2a.

ShallowNet	EEG-TCNet-Fusion	DeepNet	MCNN	CP-MixedNet	EEG-Inception	HS-CNN	Proposed CNN
40,644	17580	265,000	324,596	836,000	8,917,348	408,050	100,704

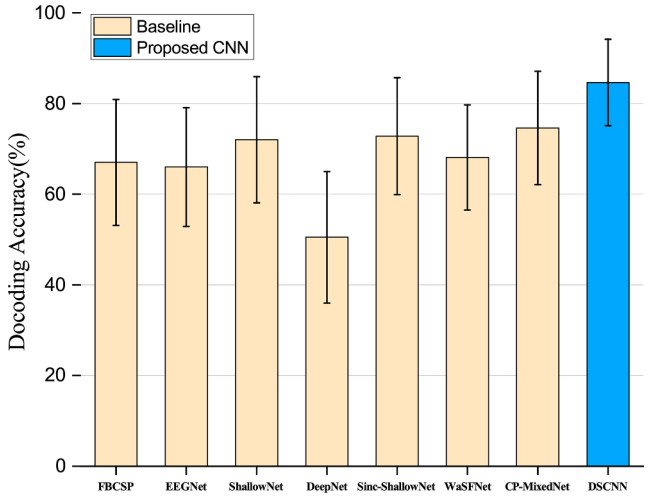

Fig. 5. Comparison of classification accuracy on four-class motor imagery dataset.

set was further split into a validation set (20% of the training set) in order to perform early stopping. Additionally, for the evaluations using 5-fold cross-validation, in each run, each specific-subject model was tested on a single additional dataset including 288 trials provided by the competition.

4. Experiment results and discussion

4.1. Dataset

In our experiments, we mainly focus on the four-class motor imagery EEG decoding task. The 2008 BCI Competition IV dataset 2a was used as public benchmark EEG dataset to evaluate the performance of the proposed model. The MI tasks include imagery of left-hand movement, right-hand movement, foot and tongue movement to be recognized. The EEG signals recorded from 9 healthy subjects. Each subject needed to perform 6 runs of different MI tasks and the number of times for each MI task is 12. Therefore, each subject finally generated 288 single EEG trials used for both train and test datasets. These EEG signals were collected by 22 electrodes corresponding to the international 10–20 system and the sampling frequency is 250 Hz. The signals have been bandpass-filtered between 0.5 Hz and 100 Hz. An additional 50 Hz notch filter was enabled to suppress line noise [37].

4.2. Learning progress

Since the left and right branches of the DSCNN can be used as independent decoding modules, in order to compare the differences between them under assembly and separation in the training process, we also trained the Branch-Left (Br-L) and the Branch-Right (Br-R) model separately. The losses and accuracies of all subjects on the test dataset were monitored during training epochs. The learning progress visualization is shown in **Fig. 2**.

Based on early stopping technique, the training of the three networks ends at different epochs. It can be found that the number of epochs required to complete the training of the Branch-Left and Branch-Right networks on the nine subjects is generally smaller than the DSCNN model. Although it can reflect that the DSCNN has a bigger complexity, especially for subject 1 and subject 9, the three networks almost finished at the same time and even the DSCNN was the first to complete the training, the DSCNN model obtained higher classification accuracy. For subject 5,6,7 and 8, the DSCNN model spent more epochs to achieve convergence, but the accuracy was greatly improved compared with the two branch networks, which means the DSCNN may acquire more features to learn and the learning efficiency is higher. Additionally, it is worth to mention that three networks all encountered different degrees of overfitting issues, but the DSCNN showed the slightest degree and this indicates that the DSCNN has more stable performance.

Furthermore, after feature aggregation, the feature maps learned by the Branch-Left accounted for much more than the another branch model in the final EEG features used for classification, because the timestep in time dimension of EEG features extracted from the Branch-Left is about more 30 times than the another. Nevertheless, the learning process of the DSCNN model is not significantly biased against one of the branch networks. This reveals the diversity and distinction between the three networks as learners of EEG features.

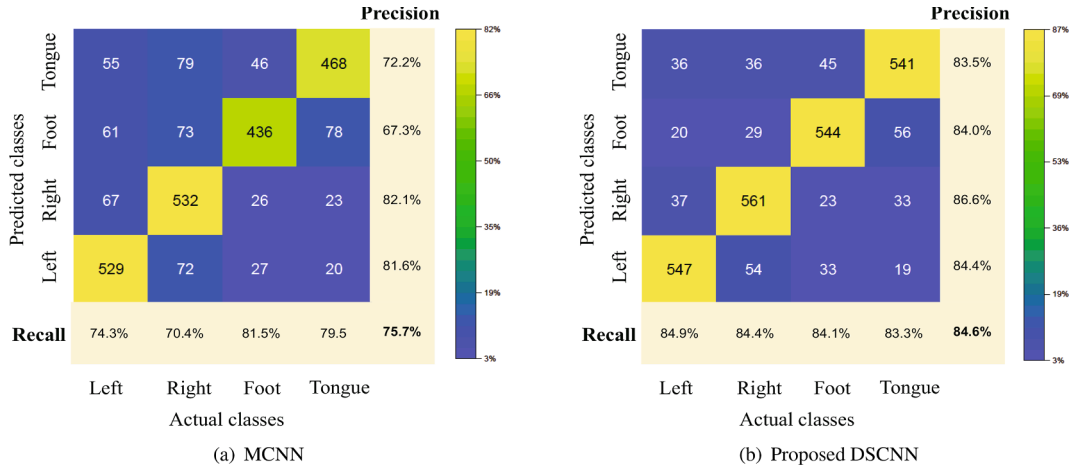

Fig. 6. The confusion matrix result of MCNN and our proposed DSCNN.

Table 5
Classification Accuracy Comparison with State-of-Art Methods.

	ShallowNet [24]	C2CM [26]	MCNN [29]	EMD-MI [39]	R-CSP [40]	Adaptive-MI [41]	MEMD-Rieman [42]	EEG-Inception* [30]	CNN-LSTM [14]	M3DCNN [19]	CSP-LCD [43]	Increment-MI [44]	AMSI-EEGNet [45]	4DDFM+ 3M3DCNN [46]	EEG-TCNet [47]	**Proposed**
S1	86.65	87.50	90.21	66.7	88.89	90.28	91.49	81.52	88.75	77.38	82.8	88.0	84.03	82.87	89.32	**92.36**
S2	62.29	65.28	63.4	63.9	51.39	57.64	60.56	78.68	65.5	60.14	65.5	66.25	55.21	**89.93**	72.44	72.22
S3	89.86	90.28	89.35	77.8	96.53	95.14	94.16	94.09	90.25	82.93	87.9	92.5	89.58	79.05	**97.44**	94.79
S4	65.61	66.67	71.16	63.2	70.14	65.97	76.72	80.48	83.5	72.29	77.6	78.25	69.79	**86.00**	75.87	81.25
S5	55.19	62.50	62.82	72.2	54.86	61.11	58.52	**79.66**	82.75	75.84	72.4	74.5	66.32	77.43	83.69	78.82
S6	48.47	45.49	47.66	70.1	71.53	65.28	68.52	76.98	74.5	68.99	70.7	58.0	61.46	**98.84**	70.69	69.79
S7	86.07	89.58	90.86	64.6	81.25	61.11	78.57	91.47	96.25	76.04	82.8	**95.5**	94.10	73.50	93.14	95.14
S8	78.41	83.33	83.72	76.4	93.75	91.67	**97.01**	91.36	87.25	76.86	87.9	88.75	85.07	67.25	86.71	89.24
S9	76.05	79.51	82.32	77.1	93.75	86.11	**93.85**	89.17	92.5	84.67	89.7	82.0	80.90	65.51	85.23	88.19
Average	72.0	74.4	75.72	70.2	78.01	74.92	79.93	**84.82**	84.58	75.02	79.7	80.42	76.27	80.04	83.84	84.64
Std. Dev.	13.9	14.5	15.24	5.92	17.01	14.54	14.99	**6.59**	9.52	7.34	8.6	12.48	12.73	10.72	9.20	9.5

* indicates that the model is trained with data augmentation and bold fonts indicate the best results.

4.3. Performance of the proposed DSCNN

4.3.1. Effectiveness of double-branch

In order to evaluate the effectiveness of the two branches Branch-Left and Branch-Right, and we also want to explore their impact on the decoding performance of the DSCNN. Therefore, we compared the performance differences between the three networks. Their decoding accuracy for each subject on the BCI IV 2a test dataset is shown in Fig. 3.

For each subject, the decoding performance of the DSCNN outperforms the two branches. Importantly, the DSCNN remarkably improves the classification accuracy of those low-performance subjects, especially for subject 2,5 and 6. In contrast with any branch model, the DSCNN improves the classification accuracy by at least 5%. In addition, the Branch-Left achieves higher accuracy than the Branch-Right on most subjects, but this advantage comes at the cost of resource consumption and bigger complexity. Table 2 reports the detailed parameters introduced by the DSCNN and each branch. Considering that the amount of trainable parameters introduced by the Branch-Left is more 6 times than the Branch-Right, this obviously shows that the Branch-Right network is much simpler while the decoding performance of the Branch-Right can still maintain a higher level for several subjects. Meanwhile, its performance competes closely with and even outperforms the Branch-Left, which is enough to explain the Branch-Right also has reliable decoding capability.

To distinguish the three networks, Wilcoxon signed-rank was applied to test the significant difference in performance between the branch models and the DSCNN. The obtained p-values are given in Table 3. It can be seen from the table that the p-values of the DSCNN for two branch models are less than 0.05 indicating that the proposed DSCNN has better performance than each branch statistically. At the same time, there is no serious dependence or bias against one branch model in decoding, which shows that the DSCNN has good independence for classification.

The Branch-Left and Branch-Right play the role of 'weak classifier' in the entire DSCNN model, therefore, their own classification performance including the diversity of feature learning ability is determined for the decoding performance of the whole DSCNN. Obviously, the DSCNN inherits the characteristics of high classification accuracy of the Branch-Left and Branch-Right, moreover, the two branch networks can make up for each other's lack of decoding performance, thereby supporting the DSCNN to obtain EEG features what a single branch network cannot extract, which promotes the DSCNN to have an excellent decoding performance.

Besides, the DSCNN model also greatly inherits the lightweight characteristics of the branch model. Fig. 4 shows the average training time across subject of different CNN models including the two branch networks, the lightweight architecture ShallowNet [24] and a moderately lightweight model MCNN [29]. Consistent with the previously listed model's size, the Branch-Left consumes the least time for training and much less than the Branch-Left, which indicates that the Branch-Right has lower complexity than the left branch. It also can be seen that the training time consumption of Branch-Left is nearly close to the shallow model ShallowNet. Also, it can be noted that the time consumption of the DSCNN is almost equal to the sum of the left and right branch network, which is lower than the multi-CNN model MCNN including four branches. This indirectly reveals that the DSCNN model has the potential to be applied in high-speed recognition scenarios.

4.3.2. Comparison with FBCSP and shallow models

In order to evaluate the performance advantages of the proposed DSCNN over the traditional algorithm and among similar CNNs, we chosen the classical FBCSP algorithm [20], EEGNet [25], ShallowNet [24], Sinc-ShallowNet [32] and WaSFNet [38]. Apart from FBCSP, these CNNs are also shallow networks as the same as our model. Additionally, two relatively deep models, DeepNet [24] and CP-MixedNet [28] are also involved in comparison. The reason ShallowNet and EEGNet are used as a baseline for comparison is that they are highly-cited open

Table 6
Mean Kappa Values of the Competing Methods.

Methods	Subjects								Average	Std	
	S1	S2	S3	S4	S5	S6	S7	S8	S9		
Ang et al. [12]	0.68	0.42	0.75	0.48	0.40	0.27	0.77	0.76	0.61	0.57	0.17
Wang et al. [48]	0.77	0.38	0.75	0.65	0.54	0.47	0.76	0.78	0.70	0.64	0.14
Zhao et al. [19]	0.70	0.46	0.79	0.60	0.54	0.65	0.54	0.70	0.71	0.64	0.10
Sakhavi et al. [26]	0.83	0.54	0.87	0.56	0.50	0.27	0.86	0.78	0.73	0.66	0.19
Amin et al. [29]	0.87	0.51	0.86	0.62	0.50	0.30	0.88	0.78	0.76	0.68	0.20
M.Riyad et al. [45]	0.79	0.40	0.86	0.60	0.55	0.49	0.92	0.80	0.74	0.68	0.18
M.Li et al. [46]	0.77	**0.87**	0.72	**0.81**	0.70	**0.98**	0.65	0.56	0.54	0.73	0.14
Majidov et al. [49]	0.80	0.55	0.80	0.75	0.72	0.61	0.81	0.78	0.77	0.74	0.09
Musallam et al. [50]	0.87	0.60	0.93	0.68	0.76	0.58	0.92	0.85	0.81	0.78	0.13
TM.Ingolfsson et al. [47]	0.86	0.63	**0.97**	0.68	0.78	0.61	0.91	0.82	0.80	0.78	0.12
R.L.Zhang et al. [14]	0.85	0.54	0.87	**0.78**	0.77	0.66	**0.95**	0.83	**0.90**	0.80	0.12
Ce.Zhang et al. [30]	0.75	0.72	0.92	0.74	0.73	0.70	0.89	**0.88**	0.86	0.80	0.08
DSCNN	**0.90**	0.63	0.93	0.75	0.72	0.60	0.94	0.86	0.84	0.79	0.13

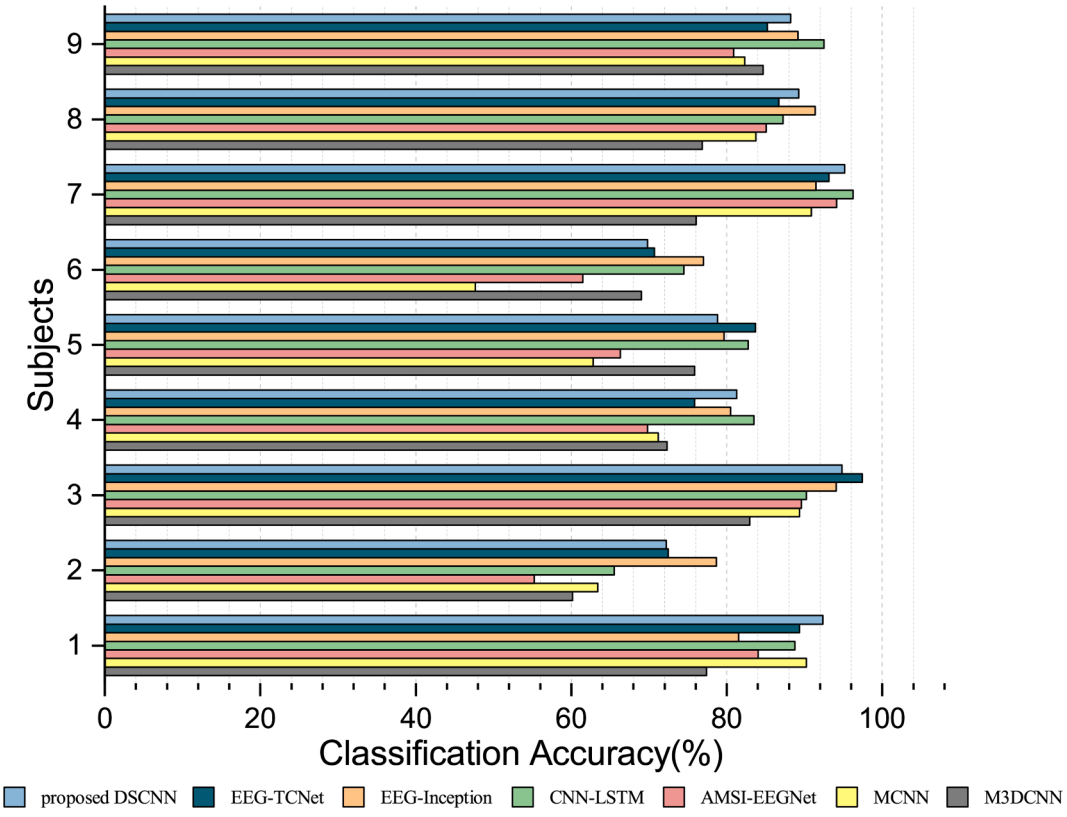

Fig. 7. Four-class within-subject decoding classification accuracy comparison with the deep, wide and fusion networks.

source models for EEG decoding and widely used. Among them, ShallowNet as a classic representative of shallow architectures, is utilized for the left branch of our DSCNN, while EEGNet also introduced depthwise separable convolution for EEG classification. Moreover, Sinc-ShallowNet and WaSFNet directly introduce an interpretable convolutional layer to maintain a lower network depth. DeepNet and CP-MixedNet are more complex than the previous lightweight architectures because they introduced more layers and modules. The amount of trainable parameters is listed in Table 4. From the table, we can see that the size of the DSCNN is only approximately one-eighth of the CP-MixedNet, its complexity is between ShallowNet and DeepNet, and it is inclined to a lightweight architecture.

The comparison result of the average decoding accuracy between the DSCNN and the baseline models is shown in Fig. 5. The error line on the bar is the standard deviation (Std). It reflects the stability of decoding across the nine subjects and the robustness of the model. As shown in the figure, the average decoding accuracy of these baseline methods generally ranges from 60% to 75% while the DSCNN outperforms all the baselines and the classification accuracy exceeds 80%, which is at least a 10% improvement. At the same time, the standard deviation of the DSCNN is the smaller, which shows the robustness of the proposed DSCNN is stronger than the other methods. Considering the size of the DSCNN model, this means it maintains a good balance between performance and complexity and the DSCNN and reaches a high decoding accuracy in similar shallow models.

4.3.3. Comparison with the state-of-the-art hybrid and wide CNN models

The adoption of feature fusion or hybrid models is a new trend in the design of decoding models or algorithms. In deep learning, a deeper and wider network can be developed by stacking or expanding network layers, or introduced hybrid models including such as CNN and RNN at the same time and extract more abundant information in the time, space

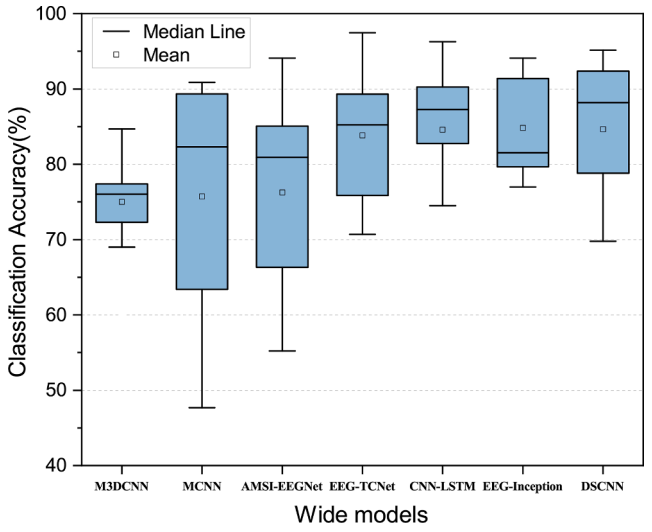

Fig. 8. Overall four-class classification performance comparison with the deep, wide and fusion networks.

and frequency domain from EEG signals. The proposed DSCNN is also extended in width, so we summarized these similar hybrid or wide CNNs and conducted a comprehensive comparison of their decoding performance with our proposed DSCNN.

For the four-class MI task, the confusion matrix including precision, recall calculated from the MCNN and DSCNN model is shown in Fig. 6. MCNN [29] is also a state-of-the-art wide network containing four branches and achieve enough satisfactory classification accuracy on the BCI IV 2a dataset. It can be seen that the DSCNN performs more balanced and stable than the MCNN for the four-class MI task, especially for decoding tasks Foot and Tongue, the classification precision of the DSCNN is 84.0% and 83.5%, respectively, which is significantly better than the MCNN. As the MCNN introduced four parallel branch networks, although which made it wider and deeper in structure, the trainable parameters introduced by it is about 3 times than the DSCNN (see Table 4). This shows the DSCNN has a higher cost performance in terms of decoding performance.

Table 5 summarizes the recent proposed methods based on traditional machine learning or deep learning, using feature fusion or introducing hybrid models, for motor imagery EEG decoding. They were all evaluated on the BCI IV 2a dataset. It can be found that the classification accuracy of most methods is concentrated between 75% and 80%, while hybrid or deep and wide models such as the CNN-LSTM, EEG-Inception, EEG-TCNet, reach nearly 84% high accuracy and have a strong robustness. Compared with these existing excellent decoding models, the proposed DSCNN has almost the close to average classification accuracy, and has advantages and disadvantages on decoding across subjects. This reveals the DSCNN is competitive with these methods.

Similarly, Table 6 mainly compares the performance of the proposed method with that of the competing fusion and deep or wide networks for four-class motor imagery EEG decoding tasks on the BCI IV 2a dataset. An additional evaluation metric kappa value was introduced for measuring the multi-classification performance of the models. It can be seen from the table the DSCNN achieves a high average kappa value of 0.79±0.13 (mean±std), and outperforms most networks, whether in terms of accuracy or robustness. In addition, we selected 6 networks including AMSI-EEGNet [45], EEG-TCNet [47], EEG-Inception [30], CNN-LSTM [14], MCNN [29] and M3DCNN [19], which cover the state-the-of-art deep, wide and fusion networks for comparison of within-subject and average decoding accuracy. The comparison result is reported in Fig. 7 and Fig. 8. According to the Fig. 7, subject 2 and 6 exhibit the worst decoding accuracies for all networks, which may be caused by the noise and artifacts. However, the proposed DSCNN still maintains a satisfactory classification accuracy around of 70% for the two low-performance subjects. For the rest subjects, the DSCNN can keep good stability on the performance, and reaches the top 3 accuracies when decoding subject 1,3,4,7,8, and 9. The proposed DSCNN is also a wide network same as the above networks. Their overall classification performance on the BCI IV 2a dataset was compared in Fig. 8. The result shows our proposed DSCNN is remarkably better than the AMSI-EEGNet, MCNN and M3DCNN, which is approximately 10% improvement. In contrast with the EEG-TCNet, EEG-Inception and CNN-LSTM with excellent performance, although the DSCNN does not completely win in performance, from the median accuracy of the nine subjects, the DSCNN is more balanced when decoding different subjects. Considering the stability of decoding across subjects and the amount of trainable parameters, the DSCNN as a shallow network is enough to compete with these complex networks. To further validate the result, Wilcoxon signed-rank test has been conducted for the 6 networks and the obtained p-values are given in Table 7. Similar to the above conclusion, the p-values of the AMSI-EEGNet, MCNN and M3DCNN are all less than 0.05, which indicates the DSCNN outperforms these networks statistically, while p-values of the rest methods reflect the DSCNN competes closely with these methods.

4.3.4. *Resource consumption and performance*

The above experimental results all show that the DSCNN has enough potential to compete with those state-of-the-art approaches. An additional consideration is that classification accuracy usually comes at the expense of model complexity such as model size, training time and resource consumption such as required memory usage when training and MACCs [47]. When these algorithms are really applied in practice, we have to take both into consideration because if high accuracy comes

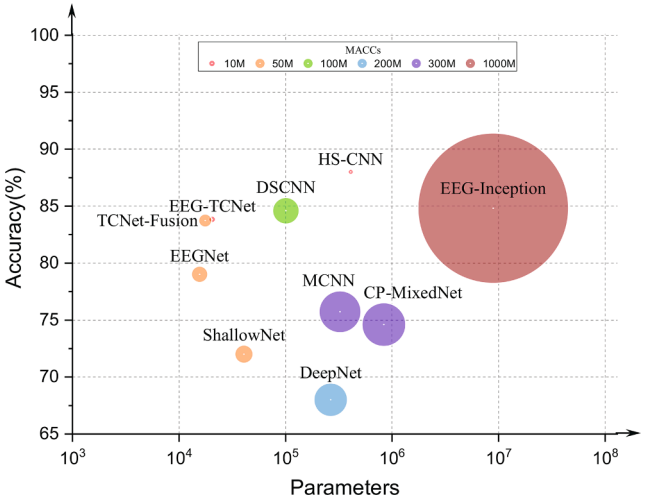

Fig. 9. Accuracy vs. parameters, size of circles ∝ MACCs. The circles are proportional to MACCs, with the corresponding legend on the top.

Table 7
Wilcoxon signed-rank test between proposed DSCNN and other deep or wide networks.

Models	EEG-Inception	CNN-LSTM	EEG-TCNet	AMSI-EEGNet	MCNN	M3DCNN
P-values	0.68	0.65	0.21	< 0.001	< 0.001	0.009

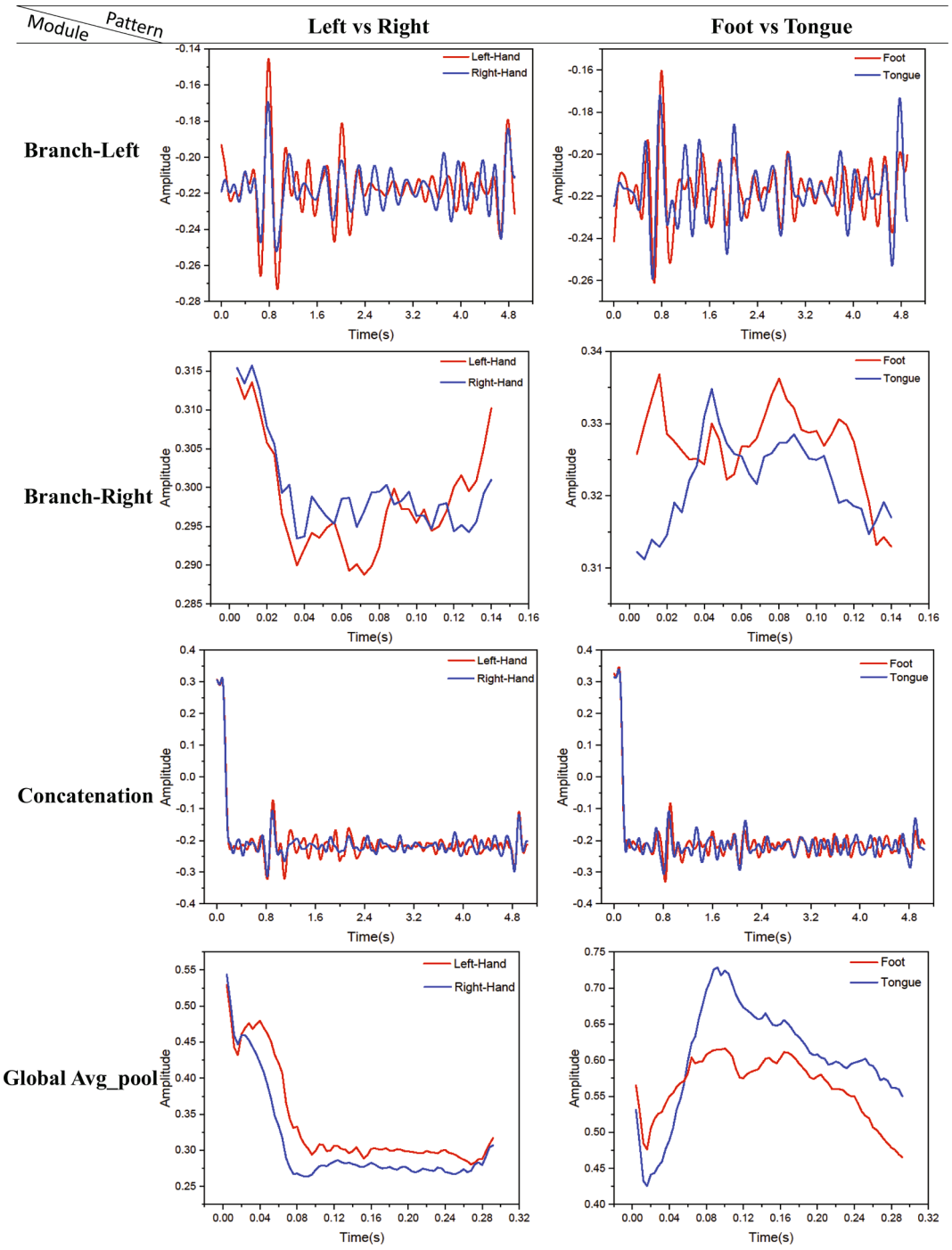

Fig. 10. The captured EEG feature signals from the two motor patterns at different intermediate stages.

at the cost of huge resource consumption, it is not friendly for BCI hardware loaded with the algorithms. Hence, we introduced MACCs as a performance metrics to explore the relationship between networks' decoding accuracy, the amount of trainable parameters and MACCs. The analysis is visualized in Fig. 9. It can be seen that although the EEG-inception model has complete advantage in decoding accuracy compared to the other models, it requires huge computing power to support it. Then MCNN, CP-MixedNet and DeepNet all require more than 200 M (million) average MACCs, which is much bigger than the lightweight architecture ShallowNet, however, the accuracy improved slightly. Obviously, the resource consumption of these models does not match their own performance. We can consider that the model falls on the position in the figure, the closer to the upper left corner, the better the comprehension performance of the model. Therefore, compared with the proposed DSCNN, it falls between HS-CNN [13] and EEG-TCNet, that is, the DSCNN is simpler than HS-CNN and the accuracy is higher than EEG-TCNet, meanwhile, it is at a lower level in terms of computing power due to its 100 M MACCs. This indicates that the DSCNN maintains a good compromise between performance and computational cost, which is much more reasonable and feasible for practical applications.

4.3.5. *Discriminative features to drive classification*

In order to evaluate whether the proposed DSCNN can be able to learn effective motor imagery EEG features for driving classification during the decoding process, we analyzed the EEG signals corresponding

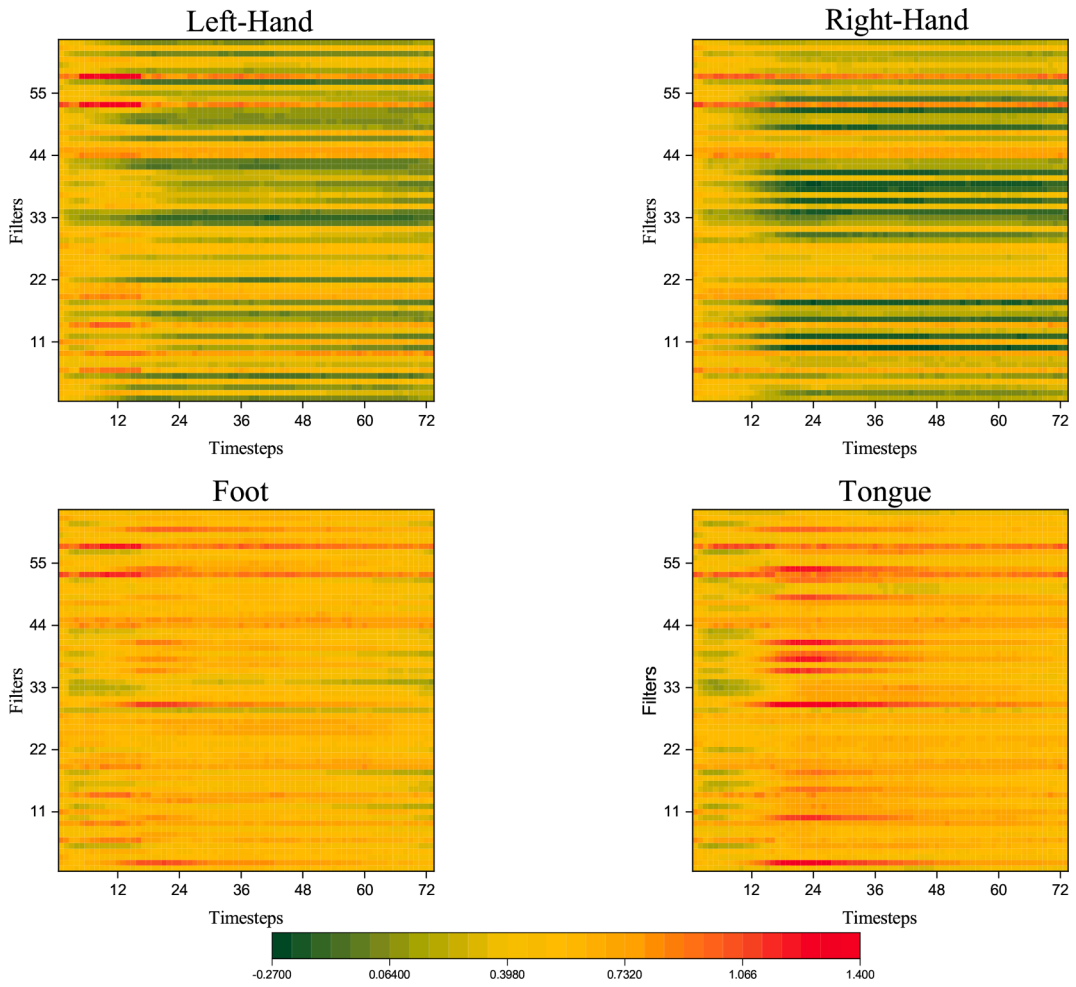

Fig. 11. The visualization results of discriminative feature signals across all subjects for 4-class MI task.

to the four classes at different intermediate stages. Fig. 10 visualizes the intermediate EEG signal series extracted by the DSCNN. These feature signals come from the left and right branch, aggregation and global average pooling layer. Remarkably, the intermediate feature representations extracted by the two branches are completely different. The Branch-Left seems to pay more attention to the details of the feature signals, which leads to retaining more time and frequency domain information. While the Branch-Right is dedicated to extracting channel dependency, the shape of the captured signals is relatively rough and simple, but it clearly distinguishes the different classification tasks especially for Left vs Right and Foot vs Tongue. This clear distinction may be due to the capture of the most essential spatial differences of the channels. Since different motor imagery tasks can activate different brain regions, for example, the C3 and C4 channels are closely related to the performing Left vs Right classification. Hence, the features captured by the DSCNN are extremely beneficial for driving the final classification. Furthermore, the different aspects of signal series captured by the left and right branches also support the independence and effectiveness of branches.

At last, the intermediate signal feature maps from the global average pooling layer are shown in Fig. 11. They are calculated from the average activation of all subjects. There are obvious differences caused by different MI tasks in these feature representations, which shows that the features captured by the DSCNN are meaningful, and the DSCNN can be able to learn the features related to the most discriminative information for motor imagery EEG classification.

5. Conclusion

In this article, we are committed to extracting more abundant features related to motor imagery EEG signals to improve the decoding accuracy for four-class MI tasks. Therefore, we proposed a shallow double-branch network including left and right branches with different structures. A series of performance comparison experiments were conducted on the BCI IV 2a dataset. The DSCNN model achieved an average classification accuracy of 85% and a high kappa score of 0.79. More importantly, in view of the requirement of quick set-up, low resource consumption and satisfactory classification accuracy for the BCI systems in practice, the proposed DSCNN model is a wide network and constrained in network depth, utilizing the width, the DSCNN has extracted more effective features and its complexity has also been greatly reduced. This makes the DSCNN maintain a good compromise between performance and resource consumption among the mainstream wide or deep and hybrid networks for EEG decoding.

CRediT authorship contribution statement

Weifeng Ma: Conceptualization, Methodology, Resources, Supervision, Project administration, Writing – review & editing. **Yifei Gong:** Methodology, Software, Investigation, Writing – original draft. **Haojie Xue:** Validation, Visualization, Data curation. **Yang Liu:** Supervision, Funding acquisition. **Xuefen Lin:** Resources, Supervision, Funding acquisition. **Gongxue Zhou:** Data curation, Validation. **Yaru Li:** Data curation, Validation.

Declaration of Competing Interest

The authors declare that they have no known competing financial interests or personal relationships that could have appeared to influence the work reported in this paper.

Acknowledgment

Our research mainly funded by the Humanities and Social Sciences Foundation of the Ministry of Education of China (20YJA880034).

References

[1] S.N. Flesher, J.E. Downey, J.M. Weiss, C.L. Hughes, A.J. Herrera, E.C. Tyler-Kabara, M.L. Boninger, J.L. Collinger, R.A. Gaunt, A brain-computer interface that evokes tactile sensations improves robotic arm control, Science 372 (6544) (2021) 831–836.
[2] C.I. Penaloza, S. Nishio, Bmi control of a third arm for multitasking, Science Robotics 3 (20).
[3] P. Kieliba, D. Clode, R.O. Maimon-Mor, T.R. Makin, Robotic hand augmentation drives changes in neural body representation, Science, Robotics 6 (54) (2021) eabd7935.
[4] X. Gu, Z. Cao, A. Jolfaei, P. Xu, D. Wu, T.-P. Jung, C.-T. Lin, Eeg-based brain-computer interfaces (bcis): A survey of recent studies on signal sensing technologies and computational intelligence approaches and their applications, IEEE/ACM Trans. Comput. Biol. Bioinf.
[5] A. Rakshit, A. Konar, A.K. Nagar, A hybrid brain-computer interface for closed-loop position control of a robot arm, IEEE/CAA J. Autom. Sin. 7 (5) (2020) 1344–1360.
[6] J.-H. Jeong, K.-H. Shim, D.-J. Kim, S.-W. Lee, Brain-controlled robotic arm system based on multi-directional cnn-bilstm network using eeg signals, IEEE Trans. Neural Syst. Rehabil. Eng. 28 (5) (2020) 1226–1238.
[7] N. Cheng, K.S. Phua, H.S. Lai, P.K. Tam, K.Y. Tang, K.K. Cheng, R.C.-H. Yeow, K. K. Ang, C. Guan, J.H. Lim, Brain-computer interface-based soft robotic glove rehabilitation for stroke, IEEE Trans. Biomed. Eng. 67 (12) (2020) 3339–3351.
[8] R. Mane, T. Chouhan, C. Guan, Bci for stroke rehabilitation: motor and beyond, J. Neural Eng. 17 (4) (2020), 041001.
[9] C. Neuper, G.R. Müller-Putz, R. Scherer, G. Pfurtscheller, Motor imagery and eeg-based control of spelling devices and neuroprostheses, Prog. Brain Res. 159 (2006) 393–409.
[10] G. Pfurtscheller, C. Brunner, A. Schlögl, F.L. Da Silva, Mu rhythm (de) synchronization and eeg single-trial classification of different motor imagery tasks, NeuroImage 31 (1) (2006) 153–159.
[11] J. Müller-Gerking, G. Pfurtscheller, H. Flyvbjerg, Designing optimal spatial filters for single-trial eeg classification in a movement task, Clin. Neurophysiol. 110 (5) (1999) 787–798.
[12] K.K. Ang, Z.Y. Chin, H. Zhang, C. Guan, Filter bank common spatial pattern (fbcsp) in brain-computer interface, in: 2008 IEEE international joint conference on neural networks (IEEE world congress on computational intelligence), IEEE, 2008, pp. 2390–2397.
[13] G. Dai, J. Zhou, J. Huang, N. Wang, Hs-cnn: a cnn with hybrid convolution scale for eeg motor imagery classification, J. Neural Eng. 17 (1) (2020), 016025.
[14] R. Zhang, Q. Zong, L. Dou, X. Zhao, Y. Tang, Z. Li, Hybrid deep neural network using transfer learning for eeg motor imagery decoding, Biomed. Signal Process. Control 63 (2021), 102144.
[15] J. Klonovs, C.K. Petersen, H. Olesen, A. Hammershoj, Id proof on the go: Development of a mobile eeg-based biometric authentication system, IEEE Veh. Technol. Mag. 8 (1) (2013) 81–89.
[16] Y. Li, W.-G. Cui, M.-L. Luo, K. Li, L. Wang, High-resolution time–frequency representation of eeg data using multi-scale wavelets, Int. J. Syst. Sci. 48 (12) (2017) 2658–2668.
[17] H.K. Lee, Y.-S. Choi, A convolution neural networks scheme for classification of motor imagery eeg based on wavelet time-frequecy image, in: 2018 International Conference on Information Networking (ICOIN), IEEE, 2018, pp. 906–909.
[18] R. Das, E. Maiorana, P. Campisi, Motor imagery for eeg biometrics using convolutional neural network, in: 2018 IEEE International Conference on Acoustics, Speech and Signal Processing (ICASSP), IEEE, 2018, pp. 2062–2066.
[19] X. Zhao, H. Zhang, G. Zhu, F. You, S. Kuang, L. Sun, A multi-branch 3d convolutional neural network for eeg-based motor imagery classification, IEEE Trans. Neural Syst. Rehabil. Eng. 27 (10) (2019) 2164–2177.
[20] K.K. Ang, Z.Y. Chin, C. Wang, C. Guan, H. Zhang, Filter bank common spatial pattern algorithm on bci competition iv datasets 2a and 2b, Front. Neurosci. 6 (2012) 39.
[21] A.S. Aghaei, M.S. Mahanta, K.N. Plataniotis, Separable common spatio-spectral patterns for motor imagery bci systems, IEEE Trans. Biomed. Eng. 63 (1) (2015) 15–29.
[22] A. Al-Saegh, S.A. Dawwd, J.M. Abdul-Jabbar, Deep learning for motor imagery eeg-based classification: A review, Biomed. Signal Process. Control 63 (2021), 102172.
[23] Y. Roy, H. Banville, I. Albuquerque, A. Gramfort, T.H. Falk, J. Faubert, Deep learning-based electroencephalography analysis: a systematic review, J. Neural Eng. 16 (5) (2019), 051001.
[24] R.T. Schirrmeister, J.T. Springenberg, L.D.J. Fiederer, M. Glasstetter, K. Eggensperger, M. Tangermann, F. Hutter, W. Burgard, T. Ball, Deep learning with convolutional neural networks for eeg decoding and visualization, Human Brain Mapping 38 (11) (2017) 5391–5420.
[25] V.J. Lawhern, A.J. Solon, N.R. Waytowich, S.M. Gordon, C.P. Hung, B.J. Lance, Eegnet: a compact convolutional neural network for eeg-based brain–computer interfaces, J. Neural Eng. 15 (5) (2018), 056013.
[26] S. Sakhavi, C. Guan, S. Yan, Parallel convolutional-linear neural network for motor imagery classification, in: 2015 23rd European Signal Processing Conference (EUSIPCO), IEEE, 2015, pp. 2736–2740.
[27] A. Farahat, C. Reichert, C.M. Sweeney-Reed, H. Hinrichs, Convolutional neural networks for decoding of covert attention focus and saliency maps for eeg feature visualization, J. Neural Eng. 16 (6) (2019), 066010.
[28] Y. Li, X.-R. Zhang, B. Zhang, M.-Y. Lei, W.-G. Cui, Y.-Z. Guo, A channel-projection mixed-scale convolutional neural network for motor imagery eeg decoding, IEEE Trans. Neural Syst. Rehabil. Eng. 27 (6) (2019) 1170–1180.
[29] S.U. Amin, M. Alsulaiman, G. Muhammad, M.A. Mekhtiche, M.S. Hossain, Deep learning for eeg motor imagery classification based on multi-layer cnns feature fusion, Future Gener. Comput. Syst. 101 (2019) 542–554.
[30] C. Zhang, Y.-K. Kim, A. Eskandarian, Eeg-inception: an accurate and robust end-to-end neural network for eeg-based motor imagery classification, J. Neural Eng. 18 (4) (2021), 046014.
[31] W. Ma, Y. Gong, G. Zhou, Y. Liu, L. Zhang, B. He, A channel-mixing convolutional neural network for motor imagery eeg decoding and feature visualization, Biomed. Signal Process. Control 70 (2021), 103021.
[32] D. Borra, S. Fantozzi, E. Magosso, Interpretable and lightweight convolutional neural network for eeg decoding: application to movement execution and imagination, Neural Networks 129 (2020) 55–74.
[33] F. Chollet, Xception: Deep learning with depthwise separable convolutions, in: Proceedings of the IEEE conference on computer vision and pattern recognition, 2017, pp. 1251–1258.
[34] D.-A. Clevert, T. Unterthiner, S. Hochreiter, Fast and accurate deep network learning by exponential linear units (elus), arXiv preprint arXiv:1511.07289.
[35] S. Ioffe, C. Szegedy, Batch normalization Accelerating deep network training by reducing internal covariate shift, in: International conference on machine learning PMLR, 2015, pp. 448–456.
[36] N. Srivastava, G. Hinton, A. Krizhevsky, I. Sutskever, R. Salakhutdinov, Dropout: a simple way to prevent neural networks from overfitting, J. Mach. Learn. Res. 15 (1) (2014) 1929–1958.
[37] C. Brunner, R. Leeb, G. Müller-Putz, A. Schlögl, G. Pfurtscheller, Bci competition 2008–graz data set a, Institute for Knowledge Discovery (v), Graz University of Technology 16 (2008) 1–6.
[38] D. Zhao, F. Tang, B. Si, X. Feng, Learning joint space–time–frequency features for eeg decoding on small labeled data, Neural Networks 114 (2019) 67–77.
[39] P. Gaur, R.B. Pachori, H. Wang, G. Prasad, An empirical mode decomposition based filtering method for classification of motor-imagery eeg signals for enhancing brain-computer interface, in: 2015 International Joint Conference on Neural Networks (IJCNN), IEEE, 2015, pp. 1–7.
[40] F. Lotte, C. Guan, Regularizing common spatial patterns to improve bci designs: unified theory and new algorithms, IEEE Trans. Biomed. Eng. 58 (2) (2010) 355–362.
[41] H. Raza, H. Cecotti, Y. Li, G. Prasad, Adaptive learning with covariate shift-detection for motor imagery-based brain–computer interface, Soft. Comput. 20 (8) (2016) 3085–3096.
[42] P. Gaur, R.B. Pachori, H. Wang, G. Prasad, A multi-class eeg-based bci classification using multivariate empirical mode decomposition based filtering and riemannian geometry, Expert Syst. Appl. 95 (2018) 201–211.
[43] Q. Ai, A. Chen, K. Chen, Q. Liu, T. Zhou, S. Xin, Z. Ji, Feature extraction of four-class motor imagery eeg signals based on functional brain network, J. Neural Eng. 16 (2) (2019), 026032.
[44] H.-J. Rong, C. Li, R.-J. Bao, B. Chen, Incremental adaptive eeg classification of motor imagery-based bci, in: 2018 International Joint Conference on Neural Networks (IJCNN), IEEE, 2018, pp. 1–7.
[45] M. Riyad, M. Khalil, A. Adib, A novel multi-scale convolutional neural network for motor imagery classification, Biomed. Signal Process. Control 68 (2021), 102747.
[46] M.-A. Li, Z.-W. Ruan, A novel decoding method for motor imagery tasks with 4d data representation and 3d convolutional neural networks, J. Neural Eng. 18 (4) (2021), 046029.
[47] T.M. Ingolfsson, M. Hersche, X. Wang, N. Kobayashi, L. Cavigelli, L. Benini, Eeg-tcnet: An accurate temporal convolutional network for embedded motor-imagery brain–machine interfaces, in: 2020 IEEE International Conference on Systems, Man, and Cybernetics (SMC), IEEE, 2020, pp. 2958–2965.
[48] H. Wang, Multiclass filters by a weighted pairwise criterion for eeg single-trial classification, IEEE Trans. Biomed. Eng. 58 (5) (2011) 1412–1420.
[49] I. Majidov, T. Whangbo, Efficient classification of motor imagery electroencephalography signals using deep learning methods, Sensors 19 (7) (2019) 1736.
[50] Y.K. Musallam, N.I. AlFassam, G. Muhammad, S.U. Amin, M. Alsulaiman, W. Abdul, H. Altaheri, M.A. Bencherif, M. Algabri, Electroencephalography-based motor imagery classification using temporal convolutional network fusion, Biomed. Signal Process. Control 69 (2021), 102826.